Am J Cancer Res 2023;13(2):419-435
www.ajcr.us /ISSN:2156-6976/ajcr0147243

Original Article

Tumor-derived Immunoglobulin-like transcript 4 facilitates angiogenesis of colorectal cancer

Jing Liu[1,2*], Fang Zhang[3*], Jie He[4], Shuyun Wang[5], Leirong Wang[5], Juan Li[3], Wenjing Shi[1], Yali Han[6], Aiqin Gao[7], Yuping Sun[5]

[1]Cheeloo College of Medicine, Shandong University, Jinan 250012, Shandong, P. R. China; [2]Department of Oncology, Affiliated Hospital of Weifang Medical University, Weifang 261031, Shandong, P. R. China; [3]Department of Oncology, Central Hospital Affiliated to Shandong First Medical University, Jinan 250013, Shandong, P. R. China; [4]Department of Oncology, People's Hospital of Zhangqiu District, Jinan 250299, Shandong, P. R. China; [5]Phase I Clinical Study Center, Shandong Cancer Hospital and Institute, Shandong First Medical University and Shandong Academy of Medical Science, Jinan 250117, Shandong, P. R. China; [6]Department of Radiation Oncology, Qilu Hospital, Cheeloo College of Medicine, Shandong University, Jinan 250012, Shandong, P. R. China; [7]Department of Thoracic Radiation Oncology, Shandong Cancer Hospital and Institute, Shandong First Medical University, Jinan 250117, Shandong, P. R. China. [*]Equal contributors and co-first authors.

Received October 25, 2022; Accepted December 24, 2022; Epub February 15, 2023; Published February 28, 2023

Abstract: Current anti-angiogenic therapies have changed the paradigm of treating colorectal cancer (CRC) patients with advanced diseases. However, the clinical response rate is still low at less than 10% due largely to complex angiogenic factors released by tumor cells. Exploring novel mechanisms of tumor angiogenesis and identifying alternative targets for combination therapies are therefore essential to effective inhibition of tumor vascularization and CRC development. Immunoglobulin-like transcript 4 (ILT4), initially identified as a suppressor of myeloid cell activity, is enriched in solid tumor cells. ILT4 favors tumor progression by inducing tumor malignant biologies as well as an immunosuppressive microenvironment. However, whether and how tumor-derived ILT4 orchestrates tumor angiogenesis is still undetermined. Here we found that tumor-derived ILT4 was positively correlated with microvessel density in CRC tissues. ILT4 induced the migration and tube formation of HUVECs *in vitro* and angiogenesis *in vivo*. Mechanistically, the activation of MAPK/ERK signaling and subsequent up-regulation of vascular endothelial growth factor-A (VEGF-A) and fibroblast growth factor 1 (FGF-1) were responsible for ILT4-induced angiogenesis and tumor progression. Importantly, ILT4 inhibition suppressed tumor angiogenesis and enhanced the efficacy of Bevacizumab treatment in CRC. Our study has identified a novel mechanism for ILT4-mediated tumor progression, which signals a new therapeutic target and alternative combination strategies to combat CRC.

Keywords: ILT4, angiogenesis, colorectal cancer, VEGF-A, FGF-1, combination therapy

Introduction

Colorectal cancer (CRC) is the third most common cancer worldwide, with rising occurrence in recent years [1]. More than 60% of CRC patients are at the stages of regional or distant metastasis when diagnosed, which is often incurable. Despite significant progress in comprehensive surgery, radiotherapy, and systemic treatment, the five-year survival rate for CRC patients with distant metastasis is merely 10-20% [2], with tumor dissemination being the major cause of cancer-related death. Therefore, it is imperative to identify novel therapeutics to prevent CRC growth and metastasis.

Angiogenesis is the key step in CRC dissemination and progression. It is reported that tumors that have reached 2-3 mm^3 volume depend on the angiogenic process for adequate oxygen and nutrients [3] and inhibiting this process can impede metastatic implantation and disease progression [4]. Based on these observations, dramatic progress has been made in CRC treatment in recent years, which targets key regulators in angiogenesis and includes drugs such as vascular endothelial growth factor (VEGF) A-targeting Bevacizumab, VEGF receptor (VEGFR) 2-targeting Ramucirumab, and multi-targeting regorafenib and fruquintinib [5]. However, the clinical response rates for these agents

remains low at no more than 10% [6]. These results imply that the mechanisms for angiogenesis are far more complex than originally thought. Consequently, identifying novel and alternative drivers for angiogenesis should provide valuable targets for CRC treatment that may be more effective at preventing CRC progression and/or metastases.

Immunoglobulin-like transcript 4 (ILT4), also named lymphocyte immunoglobulin-like receptor (LILR) B2, belongs to the Ig-like receptor superfamily [7]. It is an immunosuppressive molecule mainly expressed in myeloid immune cells including monocytes, macrophages, dendritic cells (DCs), and neutrophils [8]. In addition, ILT4 can be induced in activated T cells [9]. Upon ligation with HLA-G or Semaphorin-4A, ILT4 polarizes the M2-like phenotype of macrophages, inhibits DC maturation and neutrophil phagocytosis, and promotes Th2 differentiation, thus negatively regulating immune responses [9, 10]. Recently, we and other groups have found that ILT4 is also enriched in multiple malignant cells including acute monoblastic/monocytic leukemia (AML) cells, non-small cell lung cancer (NSCLC), breast cancer cells, and pancreatic cancer cells [11-13]. In these tumor cells, ILT4 directly promotes cell proliferation, invasion, and migration, leading to tumor progression [8, 14]. Meanwhile, ILT4 also contributes to the formation of an immunosuppressive tumor microenvironment (TME) by inducing tumor-associated macrophage M2 polarization and T cell dysfunction [15, 16]. Based on these findings, our group proposed a model in 2018 where ILT4 acts as a potential immune checkpoint for tumor immunotherapy [9].

Despite extensive studies, whether and how tumor-derived ILT4 affects tumor angiogenesis remain unknown. In the current study, we identified ILT4 as an important driver for tumor angiogenesis in CRC. We found that tumor-derived ILT4 was positively correlated with microvessel density in CRC tissues. Furthermore, ILT4 induced the migration and tube formation of human umbilical vein endothelial cells (HUVECs) *in vitro* and angiogenesis *in vivo*. Mechanistically, the activation of MAPK/ERK signaling and subsequent upregulation of VEGF-A and FGF-1 were responsible for ILT4-induced angiogenesis and tumor progression. More importantly, ILT4 inhibition reduced CRC angiogenesis and enhanced the efficacy of Bevacizumab treatment *in vivo*. Our work here not only identified a novel mechanism responsible for ILT4-mediated tumor progression but also suggests a new therapeutic target and alternative combination strategies to treat CRC.

Materials and methods

Cell culture

Human normal colonic epithelial cell line (FHC) and human CRC cell lines (HCT116, SW620, DLD-1, LoVo, HT29) were purchased from the Cell Resource Center of Chinese Academy of Sciences (Beijing, China). HT29 and HCT116 cell lines were cultured in DMEM (Gibco, Carlsbad, CA, USA) supplemented with 10% fetal bovine serum (FBS; Gibco), while FHC, SW620, LoVo, and DLD-1 cells were cultured in RPMI-1640 medium (Gibco) supplemented with 10% FBS. HUVECs were purchased from the ScienCell research laboratory (San Diego, USA) and cultured in endothelial cell medium (ECM, Sciencell, San Diego, CA, USA) supplemented with 5% FBS and 1% endothelial cell growth supplement (ECGS). HUVECs between passages 2 and 6 were used for the experiments described here.

Real-time quantitative polymerase chain reaction (RT-qPCR)

Total RNA from ILT4 overexpression or knockdown CRC cells was extracted using the RNA extraction kit (Fastagen, Shanghai, China) according to the manufacturer's instructions. After quantification, cDNA was transcribed from 1 μg of total RNA using the Evo M-MLV RT Kit (Agbio, Hunan, China). The expression of ILT4 and key angiogenesis modulators was determined by real-time qPCR using the Maxima SYBR Green qPCR Master Mix (Cwbio, Beijing, China) on the Light-Cycler 480 real-time qPCR system (Roche, Basel, Switzerland). All experiments were performed in triplicate. Amplification results were analyzed according to the 2 (-ΔΔCt) method. The specific primers used are listed in Table S1.

Western blotting

Whole cell lysates of CRC cells were prepared for western blot. Total proteins were extracted

in 1 × RIPA buffer (Cwbiotech, Beijing, China) containing proteinase and phosphatase inhibitors at 4°C and then solubilized with 5 × SDS-PAGE loading buffer (Beyotime, Shanghai, China). The samples were resolved by 10% SDS-PAGE gel and transferred onto a PVDF membrane. The membrane was incubated overnight at 4°C with appropriate primary antibodies before being washed and then incubated for 1 h with HRP-conjugated secondary antibodies at room temperature. Following automatic exposure on a chemiluminescence gel imaging system (FluorChem M, Proteinsimple, USA), signals of ILT4, VEGF-A, and key modulators of signaling pathways were normalized to those from GAPDH. The primary antibodies used here are listed in Table S2.

Immunohistochemistry staining

All experiments with human tissues were approved by the Medical Ethics Committee of Jinan Central Hospital. Paraffin-embedded primary CRC tissues (95 cases) were obtained from the Department of Pathology in Jinan Central Hospital from April 2013 to December 2015. CRC diagnosis was based on the World Health Organization criteria and staged according to the 8th edition for tumor-node-metastasis (TNM) classification of the American Joint Committee on Cancer. No preoperative antitumor treatment including chemotherapy, radiotherapy, or immunotherapy had been performed. The date for the last survival censor was May 30, 2020. Tumor sections of transplanted CRC tissues in mice were obtained at the endpoint of the animal experiments. The expression of ILT4, CD34, VEGF-A, and FGF-1 in human tissues and CD34, ERK, and pERK in mouse tissues was determined using immunohistochemical staining with the SP-9000 kit (ZSJB-Bio, Beijing, China) as we described previously [17].

Each IHC slide was independently reviewed by two pathologists with no knowledge of patient information. The slides were scored according to the following criteria: (a) proportion scores: 0 = none; 1 = less than 25%; 2 = 25-50%; 3 = 50-75%; 4 = greater than 75%; (b) intensity scores: 0 = none; 1 = weak; 2 = intermediate; 3 = strong. The final score for each patient was expressed as the product of (a) and (b). For statistical analysis, ILT4 scores of 0-5 and 6-12 in IHC analysis were considered low and high expression, respectively.

Analysis of the correlation between ILT4 and CD34 expression in the Cancer Genome Atlas (TCGA) database

The correlation of ILT4 and CD34 levels in the TCGA database was determined using the online tool GEPIA (http://gepia.cancer-pku.cn/). The Pearson correlation coefficient was used to evaluate their relationship in both colon adenocarcinoma (COAD) and rectum adenocarcinoma (READ).

ILT4 overexpression or knockdown in tumor cells and preparation of conditioned medium (CM)

Tumor cell lines with stable ILT4 overexpression (OE) or knockdown (KD) were established by the infection of lentiviruses (MOI: 5-10) (GeneChem, Shanghai, China) according to the manufacturer's instructions. The cells were selected in puromycin (Invitrogen, USA) for 48 h after lentiviral infection. The infection efficiency was >95% as determined by flow cytometry analysis of cell fluorescence.

The cells generated above were treated with inhibitors against VEGF-A (1.2 μg/ml, 6 h), FGF-1 (10 ug/ml, 48 h), ERK (U0126, 20 μM, 24 h), or NF-κB (PDTC, 10 μM, 24 h) (MCE, USA), and cultured in serum-free medium for 24 hours. The CM was then centrifuged at 3000 rpm for 10 min and harvested for ELISA, and HUVEC tubule formation and migration assays.

HUVEC migration assays

HUVEC migration was measured by the transwell migration assay. HUVECs (3×10^5 cells) resuspended in 200 μl serum-free ECM were seeded in the upper chamber of 24-well Transwell plates with 8 μm-pore polycarbonate membranes (Corning, USA). Then 600 μl of tumor CM supplemented with 10% FBS was added into the lower chamber as the chemoattractant. After 6 h at 37°C, HUVECs in the upper chamber were fixed with methanol for 30 min and stained with 0.1% Crystal Violet (Solarbio, Beijing, China) for 20 min at room temperature. The migrated cells were then counted in five randomly selected fields under

a light optic microscope (Nikon, Tokyo, Japan). Each experiment was performed in triplicate.

HUVEC tubule formation assay

Growth factor-reduced Matrigel (BD Biosciences, Franklin Lakes, NJ, USA) was liquefied at 4°C and pipetted into pre-cooled 96-well plates (60 μl/well). Plates were then incubated at 37°C for 1 hour to allow gelling. HUVECs (1.5×10^4) were resuspended in tumor CM and seeded onto the surface of the Matrigel and then cultured for 4-6 h. The number of tube-like structures was quantified under a light microscope and averaged from three randomly chosen fields for each well.

Enzyme-linked immunosorbent assay (ELISA)

The concentration of VEGF-A and FGF-1 in the tumor cell supernatant was determined by ELISA according to the manufacturer's instruction (Dakewe Biotech, Beijing, China). Briefly, 100 μl/well of CM and standards were loaded into 96-well plates and incubated with biotinylated antibodies. Then streptavidin-conjugated horseradish peroxidase (HRP) was used to visualize the reaction. OD450 values were measured using an Infinite M200 microplate reader (TECAN, Männedorf, Switzerland).

In vivo animal studies

Female BALB/c nude mice (6-8-week-old) were purchased from Beijing HFK Bioscience Co. Ltd. (Beijing, China) and maintained in the institutional animal facility. All animal studies were approved by the Institutional Animal Care Committee at Shandong University. Mice were subcutaneously injected with 4×10^6 stable ILT4-overexpressing HCT116 cells or ILT4-knockdown HT29 cells on right flanks. In CRC treatment models, 5 mg/kg clinical-grade Bevacizumab (Qilu, Pharmaceutical Co., LTD) or PBS was intraperitoneally injected into tumor-bearing mice twice a week when tumors grew to the size of 150-200 mm^3. Tumor size was measured with digital calipers every 3 days and tumor volume was calculated as 1/2 (length × $width^2$). When tumors reached the size limit (a diameter of 2 cm), mice were sacrificed and tumors were dissected and weighed. Tumor tissues were then embedded in paraffin and sectioned for further immunohistochemistry staining.

Statistical analysis

Prism 8 was used for statistical analyses. Data were expressed as means ± SD and tested by KS normality test to examine whether they were normally distributed. Student's t-test was employed for two-group comparisons if the data were fit for Gaussian distribution. The Mann-Whitney test was used for data with non-normal distribution. The correlations of ILT4 expression with clinicopathological variables were analyzed using the Chi-squared test. Survival curves were drawn using the Kaplan-Meier method and compared with the log-rank test. A P value of <0.05 was considered significant.

Results

Enriched ILT4 in CRC cells predicts increased microvessel density and poor patient survival

We first determined ILT4 gene expression in colonic epithelial (FHC) and CRC cell lines (DLD-1, SW620, HCT116, LoVo, and HT29). Compared with colonic epithelial cells, most CRC cells showed higher ILT4 gene expression (**Figure 1A**). We then confirmed these results by examining protein levels (**Figure 1B**). To further pinpoint ILT4 expression in the TME, we retrospectively collected 95 pairs of CRC tissues and their corresponding adjacent normal tissues, and examined ILT4 expression by IHC analysis. As shown in **Figure 1C** and **1D**, CRC tissues showed significantly increased ILT4 expression compared with adjacent normal tissues. Positive ILT4 staining was mainly seen in the cell membrane and cytoplasm of tumor cells (**Figure 1C**). These results clearly indicate an enrichment of ILT4 in CRC cells rather than normal epithelial cells. To further explore the significance of ILT4 expression in CRC cells, we analyzed the correlation between tumor-derived ILT4 and clinicopathological features of CRC patients. We observed that high levels of ILT4 in tumor cells were correlated with poorer cell differentiation, lymph node involvement, and advanced tumor stages (**Table 1**). In addition, patients with high ILT4 expression showed unfavorable overall survival (OS) compared to those with low ILT4 expression (**Figure 1E**). These results suggest that enriched ILT4 in CRC cells can predict poor patient outcome.

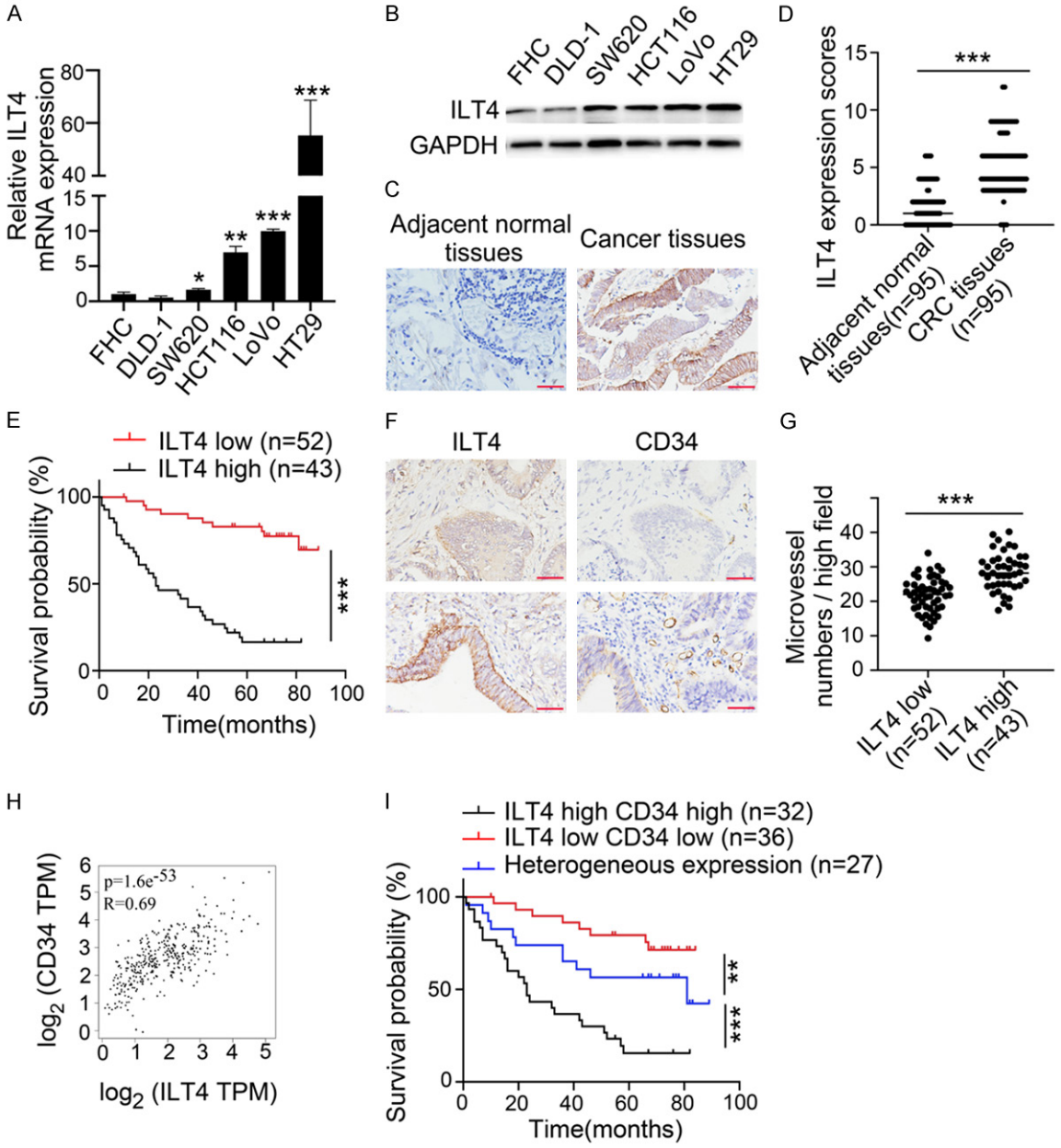

Figure 1. Enriched ILT4 in CRC cells predicts increased microvessel density and poor patient survival. (A) ILT4 gene is highly expressed in most CRC cells compared with epithelial cell line FHC by real-time qPCR analysis. The mRNA levels of ILT4 in tumor cell lines (DLD-1, SW620, HCT116, LoVo and HT29) were normalized to the relative quantity of GAPDH expression and then adjusted to that in FHC cells (served as 1). *P<0.05, **P<0.01, ***P<0.001. (B) ILT4 protein is highly expressed in most CRC cells compared with epithelial cell line FHC by western blotting. (C, D) ILT4 expression was significantly higher in CRC tissues compared with that in adjacent normal tissues by IHC analysis. (C) Showed the typical images and (D) showed the average results from 95 pairs of CRC and adjacent normal tissues. Scale bar: 20 μm. ***P<0.001. (E) Patients with high ILT4 expression showed markedly shortened OS in relative to those with low ILT4 expression. The IHC scores of <6 and ≥6 were defined as high and low ILT4 expression respectively. ***P<0.001. (F, G) CRC tissues with high ILT4 levels showed synchronously increased microvessel density, as was labelled by CD34 expression. (F) Showed the representative images and (G) showed the statistical results from 95 patients. Scale bar: 20 μm. ***P<0.001. (H) There was a significant positive correlation between ILT4 and CD34 expression in TCGA database. The online tool GEPIA was used to determine their correlation in TCGA database. (I) Patients with high ILT4 and CD34 expression showed the worst OS and patients with low ILT4 and CD34 expression had the most superior OS compared with those with heterogeneous expression. The cutoff score for high and low CD34 were the medium of microvessel number. **P<0.01, ***P<0.001.

Table 1. Correlations between ILT4 expression and clinicopathological parameters in CRC patients (n = 95)

Variables	ILT4 low (n)	ILT4 high (n)	*p*-value
Age			
>60 y	32	30	0.5181
≤60 y	19	13	
Gender			
Male	31	27	>0.9999
Female	20	16	
Differentiation			
Well and Moderate	36	21	0.0364
Poor	15	22	
Lymph node metastasis			
N0-N1	43	26	0.0109
N2-N3	8	17	
Infiltration depth			
T1-T2	6	2	0.2824
T3-T4	45	41	
TNM stage groupings			
I-II	30	15	0.0241
III-IV	21	28	
Perineural invasion			
Yes	0	11	<0.0001
No	51	32	
Distant metastasis			
M0	48	39	0.6987
M1	3	4	
Vascular invasion			
Yes	31	29	0.5264
No	20	14	

To probe the role of ILT4 in angiogenesis, we first used IHC to determine the correlation of ILT4 with microvessel density (labeled by CD34) in tumor stroma in our patient cohort (95 cases). We found that high ILT4 expression was associated with enhanced microvessel density in CRC tissues (**Figure 1F** and **1G**). We also analyzed the correlation of ILT4 with CD34 levels in the TCGA database. As shown in **Figure 1H**, there was a high positive correlation between ILT4 and CD34 levels in CRC tissues, which is consistent with findings in our patient cohort. We then grouped the CRC patients based on ILT4 and CD34 levels and analyzed the difference in survival. Clearly, patients with high ILT4 and CD34 expression in CRC tissues displayed the worst OS while those with low ILT4 and CD34 expression had the best OS, compared with the heterogeneous group (ILT4 high CD34 low or ILT4 low CD34 high) (**Figure 1I**). Collectively, these results suggest that ILT4 is highly expressed in tumor cells of CRC tissues, signaling abundant vascularization and poor patient OS.

ILT4 facilitates tumor-induced HUVEC vascularization

Given the remarkable correlation between ILT4 expression and microvessel density in CRC, we wanted to know whether ILT4 could facilitate tumor-induced angiogenesis. To this end, HUVECs were used to evaluate the vascularization ability of tumor CM *in vitro*. We first overexpressed ILT4 in CRC cell lines SW620 and HCT116, which have relatively low ILT4 levels. Using real-time qPCR and western blot, we confirmed the efficiency of ILT4 overexpression in these cells (**Figure 2A** and **2B**). We then collected CM from tumor cells with upregulated ILT4 expression and determined their effects on HUVEC migration and tubule formation. We observed that CM from ILT4-overexpressing tumor cells augmented the migration of HUVECs (**Figure 2C** and **2D**). Similarly, ILT4 overexpression in both SW620 and HCT116 increased the tumor-induced tubule formation of HUVECs (**Figure 2E** and **2F**). In the reciprocal experiment, ILT4 knockdown using lentiviral vectors encoding specific shRNAs markedly inhibited ILT4 gene and protein expression in CRC cells LoVo and HT29, which have relatively high ILT4 levels (**Figure 2G** and **2H**). In contrast to ILT4-overexpressing cells, CM from ILT4-downregulated tumor cells reduced the migration (**Figure 2I** and **2J**) and tubule formation (**Figure 2K** and **2L**) of HUVECs. These findings combined indicate that tumor-derived ILT4 facilitates tumor-induced angiogenesis *in vitro*.

ILT4 induces VEGF-A and FGF-1 expression, resulting in enhanced angiogenesis in CRC

Since angiogenesis is orchestrated by myriad canonical angiogenic factors including VEGFs, matrix metalloprotinase-9 (MMP-9), platelet-derived growth factors (PDGFs), fibroblast growth factors (FGFs), and angiopoietin-like proteins (ANGPTLs) [18], we examined their expression in ILT4-overexpressing or -knockdown tumor cells. As shown in **Figure 3A**, ILT4 overexpression upregulated VEGF-A and FGF-1

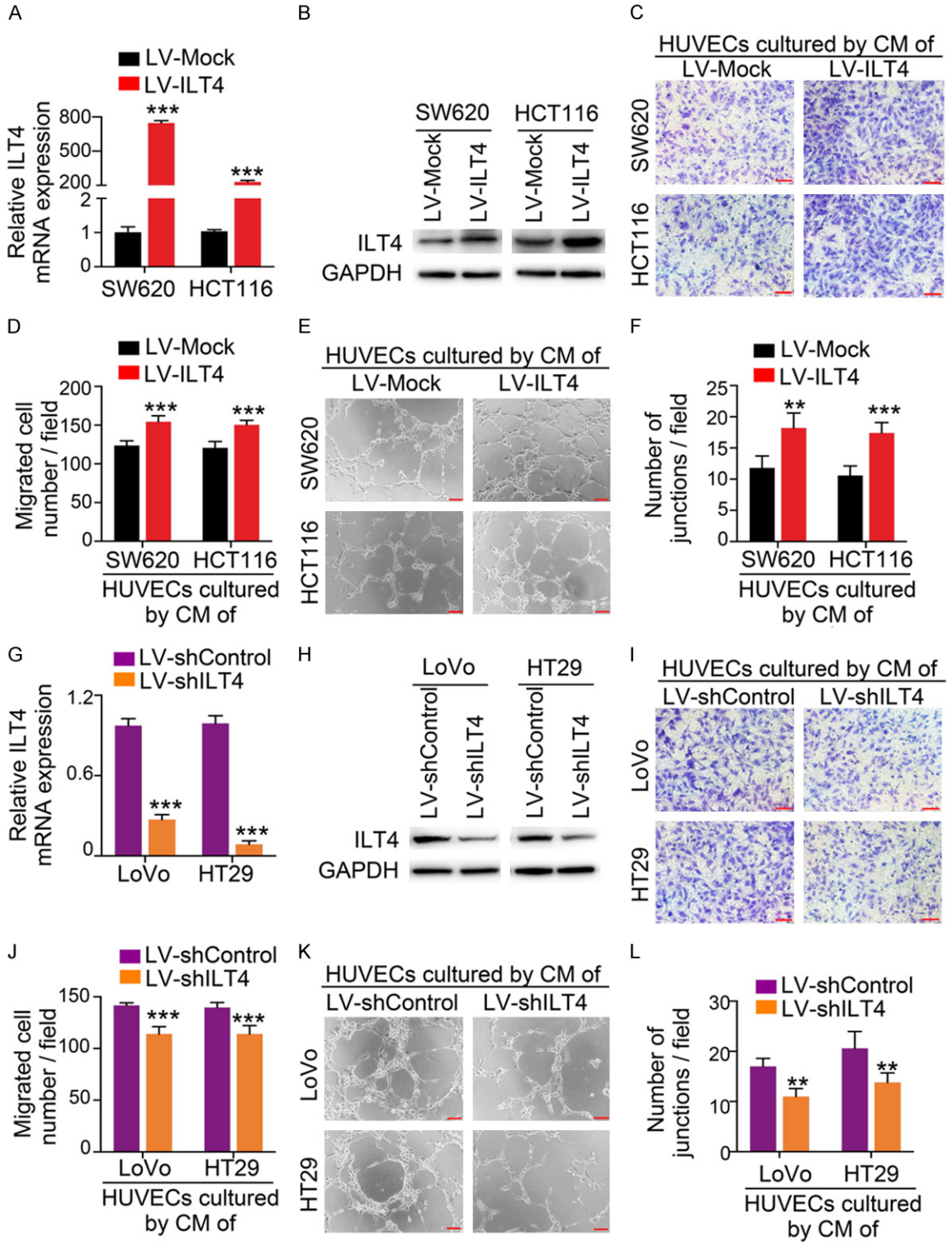

Figure 2. ILT4 facilitates tumor-induced vascularization of HUVECs. (A, B) Expression of ILT4 gene (A) and protein (B) in CRC cells (SW620 and HCT116) was markedly upregulated by infection of ILT4 vector-carrying lentivirus by real-time qPCR and western blotting analysis. ILT4 gene and protein expression were detected 48 and 72 hours after lentivirus infection respectively. ***P<0.001. (C, D) ILT4 upregulation in SW620 and HCT116 cells improved the migration ability of HUVECs induced by tumor CM by transwell assay. (C) Showed the typical images and (D) showed the average results from 5 random visual field. Scale bar: 20 μm. ***P<0.001. (E, F) CM from ILT4-upregulated SW620 and HCT116 cells stimulated more abundant tubule formation of HUVECs. (E) Showed the typical images

for tubule formation and (F) showed the total number of junctions in each well of 96-well plate. Scale bar: 20 μm. **P<0.01, ***P<0.001. (G, H) Expression of ILT4 gene (G) and protein (H) in LoVo and HT29 cells were markedly downregulated by infection of ILT4 shRNA-carrying lentivirus by real-time qPCR and western blotting analysis. ILT4 gene and protein expression were detected 48 and 72 hours after lentivirus infection respectively. ***P<0.001. (I, J) ILT4 knockdown in LoVo and HT29 cells inhibited tumor CM-induce migration of HUVECs by transwell assay. (I) Showed the typical images and (J) showed the average results from 5 random visual fields. Scale bar: 20 μm. ***P<0.001. (K, L) CM from ILT4-downregulated LoVo and HT29 cells reduced the tubule formation of HUVECs compared with that from control tumor cells. (K) Showed the typical images for tubule formation and (L) showed the total number of junctions in each well of 96-well plate. Scale bar: 20 μm. **P<0.01.

expression in both SW620 and HCT116 cells but not other angiogenic regulators examined. On the contrary, ILT4 knockdown decreased the gene expression of VEGF-A and FGF-1 bit not other regulators in both LoVo and HT29 cells (**Figure 3B**). Using western blot, we also verified ILT4-regulated VEGF-A and FGF-1 protein expression in all these tumor cell lines (**Figure 3C** and **3D**). It was reported that the secreted isoforms of VEGF-A and FGF-1 were fully processed as functional operators [19]. We therefore determined the concentration of VEGF-A and FGF-1 in the supernatant of ILT4-modulated tumor cells. As expected, ILT4 overexpression heightened VEGF-A and FGF-1 secretion in SW620 and HCT116 cells (**Figure 3E** and **3F**), while ILT4 knockdown lowered their concentration in LoVo and HT29 cells (**Figure 3G** and **3H**). To further address the effect of ILT4 on VEGF-A and FGF-1 levels in human CRC tissues, we analyzed the correlation between ILT4 and VEGF-A/FGF-1 expression in our patient cohort. We found a significant positive correlation between ILT4 and VEGF-A/FGF-1 in tumor cells from CRC tissues (**Figure 3I** and **3J**). These results indicate that ILT4 can modulate VEGF-A and FGF-1 expression and secretion in CRC cells. To further dissect the causative relationship between ILT4-induced upregulation of VEGF-A/FGF-1 and tumor angiogenesis, we used VEGF-A and FGF-1 neutralizing antibodies to block VEGF-A/FGF-1 in the CM from ILT4-overexpressing SW620 and HCT116 cells, and examined how that affected HUVEC migration and tubule formation. Consistent with the results in **Figure 2**, overexpressing ILT4 markedly promoted the migration of HUVECs induced by tumor CM (**Figure 3K** and **3L**). However, when VEGF-A or FGF-1 was blocked, enhanced HUVEC migration with ILT4 overexpression was significantly inhibited (**Figure 3K** and **3L**). Likewise, ILT4 overexpression increased tumor-induced tubule formation of HUVECs, which was blocked when VEGF-A and FGF-1 were neutralized (**Figure 3M** and **3N**). Collectively, these studies underline VEGF-A and FGF-1 as crucial mediators of ILT4-induced angiogenesis in CRC.

ILT4 controls VEGF-A and FGF-1 production and tumor angiogenesis by activating MAPK/ERK signaling

We next explored in tumor cells downstream signaling events of ILT4-mediated enhancement of VEGF-A and FGF-1 production and angiogenesis. Previous studies have shown that ILT4 in tumor cells or DCs can activate MAPK/ERK, mTOR, or NF-κB signaling to perform its biological functions [8, 20]. Therefore, we selected these pathways for our subsequent study. We first detected the phosphorylation of these pathway modulators in ILT4-overexpressing SW620 and HCT116 cells. As shown in **Figure 4A**, overexpression of ILT4 selectively activated the phosphorylation of NF-κB and MAPK/ERK in both cell lines. Moreover, ILT4 knockdown in LoVo and HT29 cells reduced their phosphorylation (**Figure 4B**). Next, we sought to explore whether VEGF-A and FGF-1 were controlled by the activation of these two signaling pathways using specific pharmacological inhibitors to their signaling in ILT4-overexpressing SW620 and HCT116 cells. We found that ILT4 overexpression upregulated the expression of VEGF-A and FGF-1 and activated the phosphorylation of NF-κB and MAPK/ERK. However, inhibition of MAPK/ERK but not NF-κB prevented ILT4-dependent VEGF-A/FGF-1 expression (**Figure 4C**). Unsurprisingly, inhibition of MAPK/ERK rather than NF-κB reversed ILT4-upregulated VEGF-A and FGF-1 secretion into the supernatant (**Figure 4D** and **4E**). We also assessed the effects of MAPK/ERK and NF-κB inhibitors on HUVEC migration and tubule formation. As expected, ILT4 overexpression promoted tumor CM-induced HUVEC migration and tubule formation. However, blocking MAPK/ERK signaling rather than NF-κB prevented ILT4-

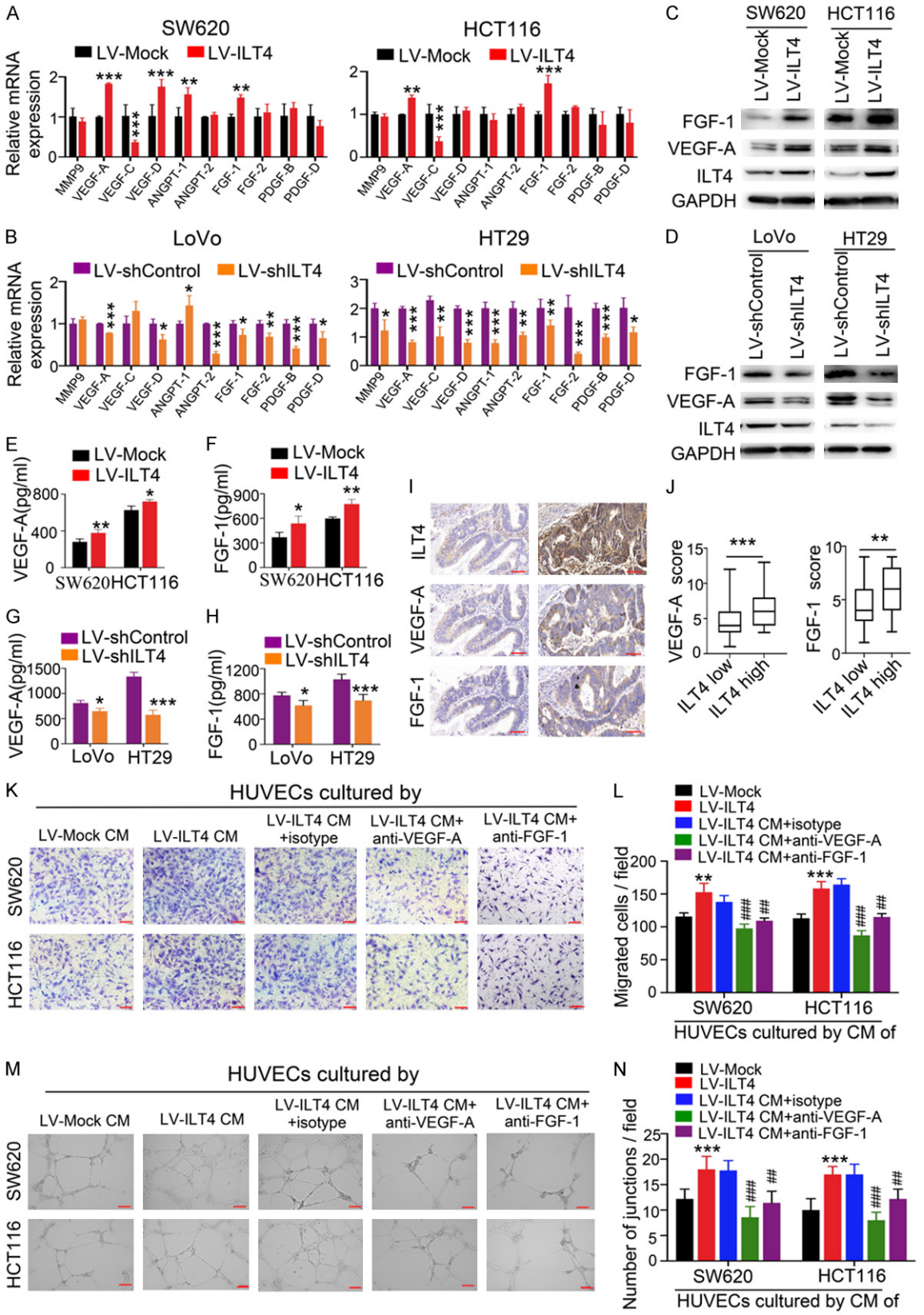

Figure 3. ILT4 induces VEGF-A and FGF-1 expression, resulting to enhanced angiogenesis in CRC. (A) ILT4 overexpression in SW620 and HCT116 upregulated the expression of VEGF-A and FGF-1 rather than other angiogenic regulators by real-time qPCR analysis. The gene expression of canonical angiogenic regulators (including MMP-9,

VEGF-A, VEGF-C, VEGF-D, ANGPT-1, ANGPT-2, FGF-1, FGF-2, PDGF-B and PDGF-D) was determined 48 hours after lentivirus infection. **P<0.01, ***P<0.001. (B) ILT4 knockdown in LoVo and HT29 decreased the expression of VEGF-A and FGF-1 rather than other angiogenic regulators by real-time qPCR analysis. The gene expression of canonical angiogenic regulators (including MMP-9, VEGF-A, VEGF-C, VEGF-D, ANGPT-1, ANGPT-2, FGF-1, FGF-2, PDGF-B and PDGF-D) was determined 48 hours after lentivirus infection. *P<0.05, **P<0.01, ***P<0.001. (C) ILT4 overexpression in SW620 and HCT116 increased the protein level of VEGF-A and FGF-1 expression while (D) ILT4 knockdown in LoVo and HT29 decreased VEGF-A and FGF-1 expression by western blotting analysis. The expression of ILT4, VEGF-A and FGF-1 was examined 72 hours after lentivirus infection. (E-H) The CM from ILT4-overexpressed/downregulated tumor cells was collected to determine the concentration of VEGF-A and FGF-1 by ELISA. ILT4 overexpression in SW620 and HCT116 elevated VEGF-A and FGF-1 secretion (E, F) while ILT4 knockdown in LoVo and HT29 suppressed VEGF-A and FGF-1 secretion (G, H) into the supernatant of tumor cells. *P<0.05, **P<0.01, ***P<0.001. (I, J) ILT4 expression in tumor cells was positively correlated with that of VEGF-A and FGF-1 in CRC tissues by IHC analysis. (G) Showed the representative images of ILT4 and VEGF-A/FGF-1 expression, while (H) displayed the summarized results from 95 patient samples. Scale bar: 20 μm. ***P<0.001. (K, L) CM from ILT4-overexpressed HCT116 and SW620 cells augmented the migration of HUVECs. However, VEGF-A/FGF-1 blockade reversed ILT4 overexpression-induced HUVEC migration. (K) Showed the typical images of HUVEC migration by transwell assay, and (L) showed the average results from 5 random fields in each group. Scale bar: 20 μm. **P<0.01, ***P<0.001 compared with LV-Mock group. ###P<0.001 compared with LV-ILT4 CM+isotype group. (M, N) CM from ILT4-overexpressed HCT116 and SW620 cells promoted the tubule formation of HUVECs, while blockade of VEGF-A/FGF-1 prevented ILT4-overexpression increased tubule formation of HUVECs. (K) Showed the typical images of HUVEC tubule formation, and (L) showed the total number of junctions in each group. Scale bar: 20 μm. ***P<0.001 compared with LV-Mock group. ### P<0.001 compared with LV-ILT4 CM+isotype group.

upregulated HUVEC migration (**Figure 4F** and **4G**) and tubule formation (**Figure 4H** and **4I**). Taken together, these results clearly indicate that ILT4-activated MAPK/ERK signaling is responsible for VEGF-A and FGF-1 production and tumor angiogenesis in CRC.

ILT4 promotes tumor angiogenesis and progression in vivo

Our results thus far demonstrated ILT4-induced tumor angiogenesis and development via activated MAPK/ERK signaling and the resultant production of VEGF-A and FGF-1. Next we wanted to explore whether ILT4 was critical for controlling tumor angiogenesis and progression *in vivo*. We established tumor transplantation models using immunodeficient BALB/c nude mice to determine how tumor-derived ILT4 would affect CRC growth and angiogenesis. Approximately 4×10^6 ILT4-overexpressing HCT116 cells or ILT4-knockdown HT29 cells were subcutaneously inoculated into the right flanks of nude mice. Tumor size was evaluated every 3 days. At the end of the experiments, tumors were isolated and weighed and tumor tissues were embedded in paraffin and sectioned for IHC staining. Our results showed that ILT4 overexpression markedly accelerated tumor growth in nude mice (**Figure 5A**). Furthermore, tumors collected 30 days post tumor inoculation from the ILT4-overexpressing group were significantly larger than those from the control group (**Figure 5B**). In addition, we obtained consistent results of the average tumor weights between the two groups (**Figure 5C**). Given our results above showing VEGF-A/FGF-1 upregulation and MAPK/ERK activation contributing to ILT4-promoted tumor angiogenesis *in vitro*, we next validated this correlation in transplanted tumor tissues. As indicated in **Figure 5D-F**, tumor tissues in the ILT4-overexpressing group displayed significantly enhanced microvessel densities and MAPK/ERK phosphorylation compared with those in the control group. These studies suggest that ILT4 activates MAPK/ERK signaling and promotes tumor angiogenesis, resulting in accelerated tumor growth.

To further validate this conclusion, we established a similar tumor transplantation model using ILT4-downregulated HT29 cells to determine the effect of ILT4 knockdown on tumor growth and angiogenesis. As predicted, ILT4 knockdown in HT29 cells slowed tumor growth in nude mice (**Figure 5G**). Meanwhile, the ILT4 knockdown group displayed substantially decreased tumor size (**Figure 5H**) and weight (**Figure 5I**). We next determined the microvessel densities and level of phosphorylated ERK, and observed markedly diminished microvessel density and MAPK/ERK activation in the ILT4 knockdown group relative to the control group (**Figure 5J-L**). Taken together, these results indicate that ILT4 is a strong promoter of tumor angiogenesis, and knockdown of ILT4 may be an effective strategy to suppress tumor angiogenesis and progression.

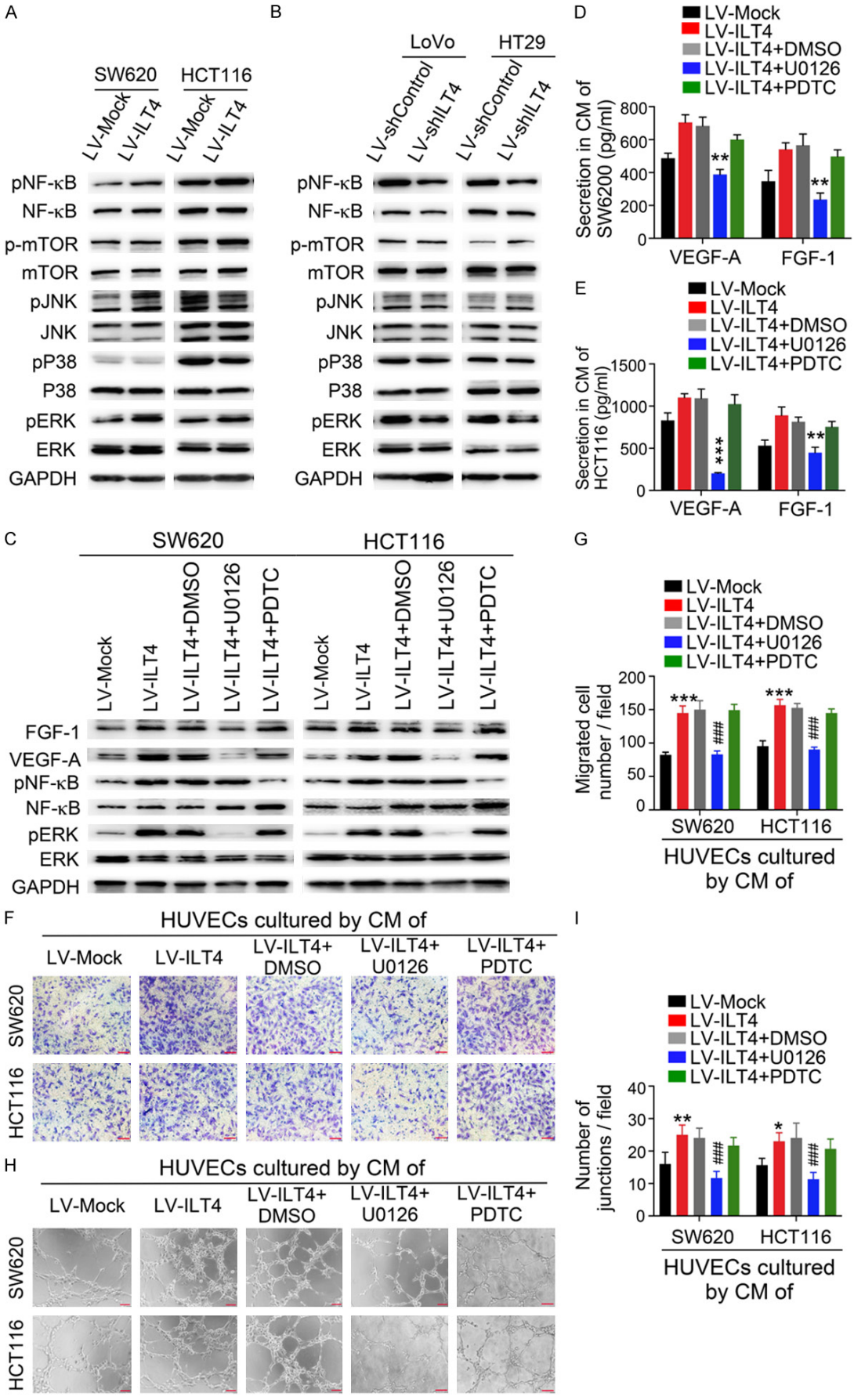
A
SW620
HCT116
LV-Mock
LV-ILT4
LV-Mock
LV-ILT4
pNF-κB
NF-κB
p-mTOR
mTOR
pJNK
JNK
pP38
P38
pERK
ERK
GAPDH
B
LoVo
HT29
LV-shControl
LV-shILT4
LV-shControl
LV-shILT4
pNF-κB
NF-κB
p-mTOR
mTOR
pJNK
JNK
pP38
P38
pERK
ERK
GAPDH
D
LV-Mock
LV-ILT4
LV-ILT4+DMSO
LV-ILT4+U0126
LV-ILT4+PDTC
Secretion in CM of SW6200 (pg/ml)
800
600
400
200
0
**
**
VEGF-A
FGF-1
E
LV-Mock
LV-ILT4
LV-ILT4+DMSO
LV-ILT4+U0126
LV-ILT4+PDTC
Secretion in CM of HCT116 (pg/ml)
1500
1000
500
0
***
**
VEGF-A
FGF-1
C
SW620
HCT116
LV-Mock
LV-ILT4
LV-ILT4+DMSO
LV-ILT4+U0126
LV-ILT4+PDTC
LV-Mock
LV-ILT4
LV-ILT4+DMSO
LV-ILT4+U0126
LV-ILT4+PDTC
FGF-1
VEGF-A
pNF-κB
NF-κB
pERK
ERK
GAPDH
G
LV-Mock
LV-ILT4
LV-ILT4+DMSO
LV-ILT4+U0126
LV-ILT4+PDTC
Migrated cell number / field
200
150
100
50
0
***
***
###
###
SW620
HCT116
HUVECs cultured by CM of
F
HUVECs cultured by CM of
LV-Mock
LV-ILT4
LV-ILT4+ DMSO
LV-ILT4+ U0126
LV-ILT4+ PDTC
SW620
HCT116
I
LV-Mock
LV-ILT4
LV-ILT4+DMSO
LV-ILT4+U0126
LV-ILT4+PDTC
Number of junctions / field
40
30
20
10
0
**
*
###
###
SW620
HCT116
HUVECs cultured by CM of
H
HUVECs cultured by CM of
LV-Mock
LV-ILT4
LV-ILT4+ DMSO
LV-ILT4+ U0126
LV-ILT4+ PDTC
SW620
HCT116

Figure 4. ILT4 controls VEGF-A and FGF-1 production and tumor angiogenesis via activation of MAPK/ERK signaling. (A) ILT4 overexpression in SW620 and HCT116 activated the phosphorylation of ERK and NF-κB signaling rather than JNK, P38 and mTOR signaling. SW620 and HCT116 cells were transfected with ILT4 vector-carrying lentivirus for 72 hours and phosphorylation of ERK, JNK, P38, mTOR and NF-κB was determined by western blotting. (B) Knockdown of ILT4 in LoVo and HT29 cells inhibited the phosphorylation of ERK and NF-κB signaling but not JNK, P38 and mTOR signaling. LoVo and HT29 cells were transfected with ILT4 shRNA-carrying lentivirus for 72 hours and phosphorylation of ERK, JNK, P38, mTOR and NF-κB was determined by western blotting. (C) Treatment of tumor cells with U0126 rather than with PDTC reversed ILT4 overexpression-induced VEGF-A and FGF-1 expression. ILT4-overexpressed tumor cells were treated with the specific inhibitors for ERK (U0126) or NF-κB (PDTC) for 24 hours, and the levels of pERK, pNF-κB, VEGF-A and FGF-1 were examined by western blotting. (D, E) Inhibition of ERK rather than NF-κB reversed ILT4 overexpression-elevated VEGF-A and FGF-1 secretion. SW620 (D) and HCT116 (E) cells with ILT4 overexpression were treated by U0126 or PDTC for 24 hours, then the medium was replaced by serum-free medium and cells were cultured for another 24 hours. The CM was collected to determine the concentration of VEGF-A and FGF-1 by ELISA. **P<0.01 compared with LV-Mock group. ###P<0.001 compared with LV-ILT4+DMSO group. (F, G) Inhibition of ERK rather than NF-κB prevented ILT4 overexpression-promoted HUVECs migration. The same CM as in (D) was used for treatment of HUVECs and their migration ability was determined using transwell assay. (F) Showed the typical images of migrated HUVECs, and (G) showed the average of migrated cells from 5 random fields. Scale bar: 20 μm. ***P<0.001 compared with LV-Mock group. ###P<0.001 compared with LV-ILT4+DMSO group. (H, I) Inhibition of ERK rather than NF-κB inhibited ILT4 overexpression-augmented tubule formation of HUVECs. The same CM as in (D) was used to induce the tubule formation of HUVECs. (H) Showed the typical images of HUVEC tubule formation, and (I) showed the total number of junctions in each group. Scale bar: 20 μm. *P<0.05, **P<0.01, compared with LV-Mock group. ###P<0.001 compared with LV-ILT4+DMSO group.

ILT4 blockade enhanced the anti-tumor activity of Bevacizumab in vivo

Bevacizumab is the first-line selection for anti-angiogenetic treatment in the clinical practice of CRC treatment. However, its benefit is limited due to the single-target effect. Exploring combination treatment to block multiple targets is crucial to overcoming Bevacizumab resistance. To verify the impact of ILT4 blockade on Bevacizumab efficacy, we established CRC treatment models using immunodeficient BALB/c nude mice inoculated with ILT4-knockdown or control HT29 cells. When tumors grew to 150-200 mm^3 in size, mice were treated with twice per week peritoneal injection of 5 mg/kg Bevacizumab. We found that both ILT4 blockade and Bevacizumab slowed tumor growth individually in mice, and the combined treatment generated a significant synergistic effect on tumor growth (**Figure 6A**). Final tumor sizes and weights confirmed the above results (**Figure 6B** and **6C**). To further verify their synergy on tumor angiogenesis and the underlying mechanism, we determined the expression of CD34 and pERK in tumors from each group. As shown in **Figure 6D** and **6E**, both ILT4 inhibition and Bevacizumab decreased the expression of CD34, as well as the phosphorylation of ERK in tumor cells, while the combination treatment displayed the most dramatic effect. We also examined blood vessel density in tumor tissues from each group. Similarly, Bevacizumab and ILT4 inhibition alone each decreased the vasculization in tumor tissues with the most significant effect seen in the combination group (**Figure 6F**). Collectively, these results clearly indicate that ILT4 inhibition can enhance the anti-tumor activity of Bevacizumab thanks to the synergetic inhibition of tumor angiogenesis.

Discussion

Colorectal cancer (CRC) is among the most lethal and prevalent malignancies worldwide. It has been reported that half of all CRC patients develop metastatic diseases, with a five-year survival rate of ~12% [21]. For this subpopulation, anti-angiogenesis therapies have become the standard systematic treatment to suppress tumor progression [22]. However, anti-angiogenic therapies in CRC lead only to modest clinical benefits with no more than 10% response rate [6]. More importantly, resistance invariably develops after a short duration of improvement [5, 22]. Mechanistically, compensatory activation of other signaling pathways and alternative secretion of angiogenesis-related proteins represent the main cause of resistance to anti-angiogenic agents [23]. Therefore, identifying alternative mechanisms for tumor vasculature establishment and combinatorial target inhibition is urgently needed to overcome current limitation in anti-angiogenic therapies. In this study, we identified ILT4 as a novel driver for tumor angiogenesis. Furthermore, we demonstrated that the activation of

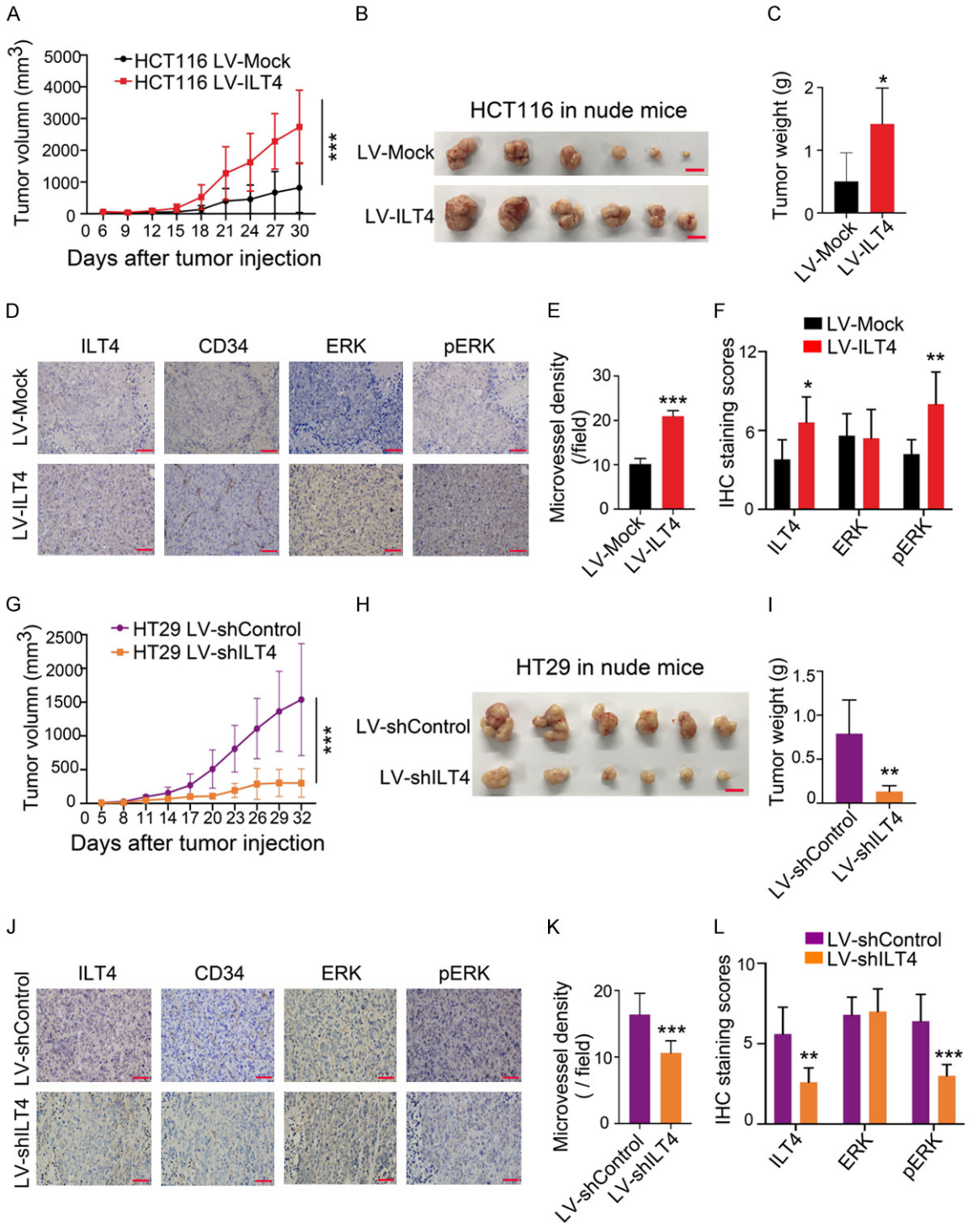

Figure 5. ILT4 promotes tumor angiogenesis and progression in *vivo*. (A) Overexpression of ILT4 in HCT116 accelerated the growth of transplanted tumors in nude mice. 4 × 10^6 ILT4-overexpressing or control HCT116 cells were subcutaneously injected into the right flanks of BALB/c nude mice, and tumor size was measured every 3 days. ***P<0.001. (B, C) ILT4 overexpression yield remarkably larger tumor size and weight compared with control group. (B) showed the final tumor image in each mouse and (C) showed the average tumor weight in each group at the end point of the experiment. Scale bar: 1 cm. *P<0.05. (D-F) Tumor tissues in ILT4-overexpression group displayed increased microvessel density and ERK phosphorylation compared with those in control group by IHC analysis. (D) Showed the representative images of IHC. (E) Showed the statistical results of microvessel density from 6 mice in the LV-Mock group and LV-ILT4 group. (F) Showed the statistical results of ILT4, ERK and pERK from 6 mice of each group. *P<0.05, **P<0.01, ***P<0.001. (G) ILT4 knockdown in HT29 slowed down the growth of transplanted

tumors in nude mice. 4 × 10^6 ILT4-downregulated or control HT29 cells were subcutaneously injected into the right flanks of BALB/c nude mice, and tumor size was measured every 3 days. ***P<0.001. (H, I) ILT4 knockdown yield significantly smaller tumor size and weight compared with control group. (H) showed the final tumor image in each mouse and (I) showed the average tumor weight in each group at the end point of the experiment. Scale bar: 1cm. **P<0.01. (J-L) Tumor tissues in ILT4-knockdown group displayed decreased microvessel density and ERK phosphorylation compared with those in control group by IHC analysis. (J) Showed the representative images of IHC and (K) showed the statistical results of microvessel density from 6 mice in each group. (L) Showed the statistical results of ILT4, ERK and pERK from 6 mice of each group. **P<0.01, ***P<0.001.

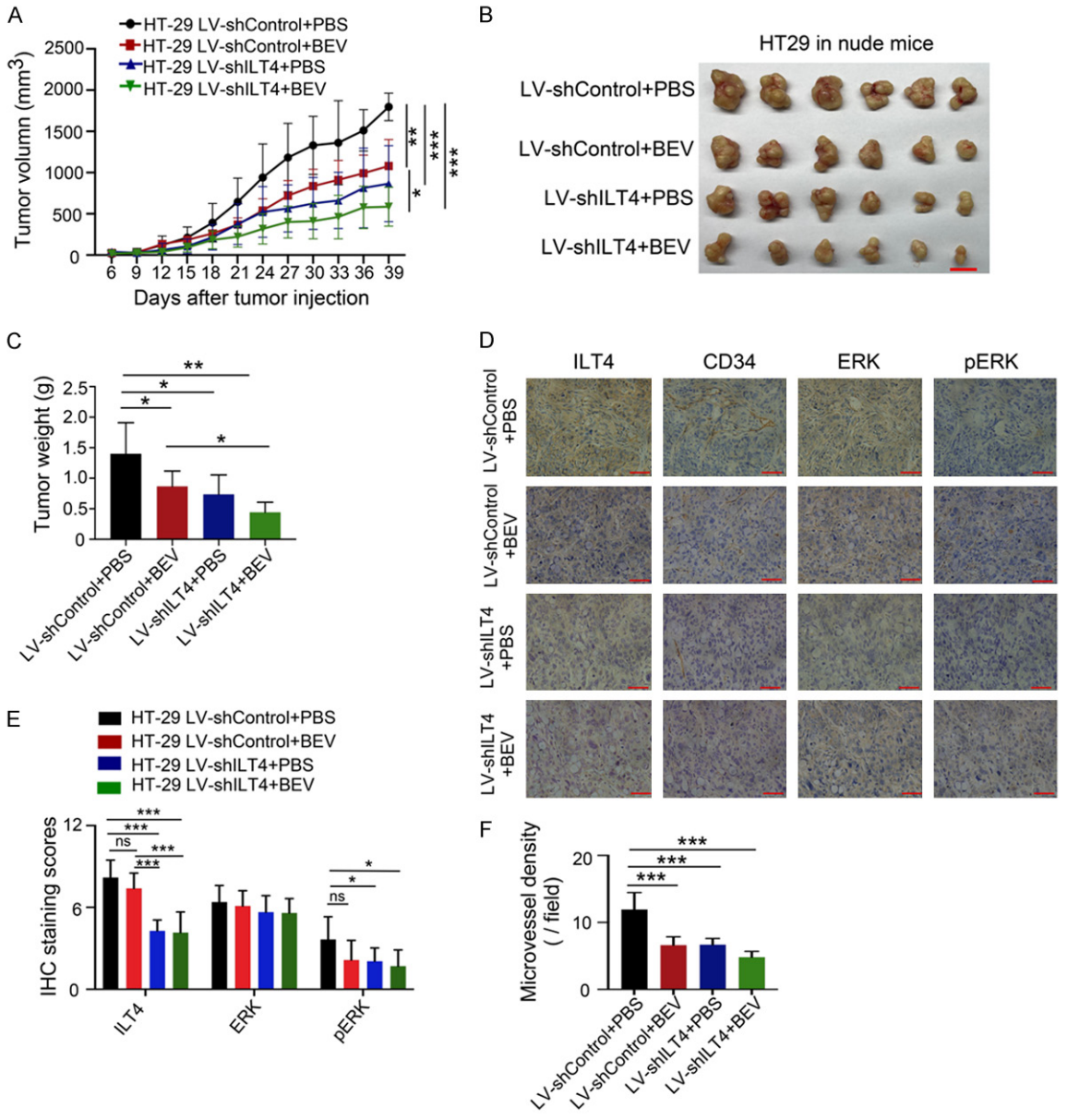

Figure 6. ILT4 blockade enhanced the anti-tumor activity of Bevacizumab *in vivo*. (A-C) Both ILT4 blockade and Bevacizumab slowed down tumor growth in mice, while combined treatment generated a significant synergistic effect on tumor growth. Immunodeficient BALB/c nude mice were inoculated with ILT4-knockdown or control HT29 cells. When tumors grew to a size of 150-200 mm^3, 5 mg/kg Bevacizumab was intraperitoneally injected into tumor-bearing mice twice a week. Tumor size was evaluated every 3 days. At the end of the experiments, tumors were isolated from the sacrificed mice and weighed. (A) Showed the growth curve in each group, (B) and (C) showed the final tumor size and weight respectively. *P<0.05, **P<0.01, ***P<0.001. BEV, Bevacizumab. (D, E) While both ILT4 inhibition and Bevacizumab decreased the expression of CD34 and ERK phosphorylation in tumor cells, combination treatment displayed the most remarkable inhibition. The final tumor tissues were embedded in paraffin and IHC staining

were performed to determined the expression of CD34 and pERK. (D) Showed the representative images for IHC staining and (E) showed the average results from 6 mice of each group. *P<0.05, **P<0.01, ***P<0.001; ns, no significance; BEV, Bevacizumab. (F) Bevacizumab and ILT4 inhibition decreased the microvessel density in tumor tissues compared with control groups, while combined application of Bevacizumab and ILT4 inhibition generated the least microvessel density in tumor tissues. Microvessels were labled by CD34 and calculated by CD34 positive tubular structure. ***P<0.001.

MAPK/ERK signaling and subsequent upregulation of VEGF-A and FGF-1 were responsible for ILT4-induced angiogenesis and tumor progression. Importantly, ILT4 inhibition reduced tumor angiogenesis and growth and enhanced the efficacy of Bevacizumab in CRC *in vivo*.

ILT4 was initially reported to be expressed in myeloid cells and function as an immune suppressor [24]. In the last decade, we and other groups have found ILT4 to be enriched in tumor cells of AML, NSCLC, breast cancer, and pancreatic cancer, which predicts unfavorable patient survival [8]. These results point to ILT4 as a negative prognostic biomarker in multiple solid tumors and are consistent with our current findings in CRC. Mechanistically, ILT4 directly promotes tumor cell renewal, proliferation, and migration and invasion, which supports ILT4 as a crucial tumor driver [25-27]. More recently, we identified tumor-derived ILT4 as a modulator of T cell immunity that can induce tumor-specific T cell dysfunction directly and M2-like polarization of TAMs indirectly, creating an immunosuppressive TME for tumor progression [15, 16]. These findings have contributed to a more comprehensive understanding of ILT4-orchestrated tumor promotion. However, whether tumor-derived ILT4 plays a role in tumor-mediated angiogenesis and the underlying mechanisms remains undefined. Here, for the first time, we uncovered the potential role of ILT4 in tumor angiogenesis and propose ILT4 as a novel target for blocking tumor vascularization and progression. Furthermore, we validated our results in a preclinical CRC model and observed the profound impact of ILT4 inhibition on tumor angiogenesis and growth. More importantly, through synergetic inhibition of ILT4 with Bevacizumab, we explored a novel combination therapy that can improve the efficacy and response duration of Bevacizumab, which should help overcome drug resistance.

Angiogenesis is controlled by multiple pro-angiogenic factors produced by various cell types in the TME, including tumor cells, macrophages, endothelial cells, and tumor-associated stroma [28]. Tumor-derived VEGFs, PDGFs, FGFs, and ANGPTLs are among the most critical growth factors for tumor vascularization [29]. Here, using gain- and loss-of-function strategies, we explored the mechanism for ILT4-regulated angiogenesis in CRC and identified VEGF-A and FGF-1 as the main mediators. It is well accepted that VEGF-A induces the growth, migration, and differentiation of endothelial cells, thus facilitating angiogenesis in solid tumors, and acts as a key driver for angiogenesis [31]. The evidence strongly supports a role of ILT4 in tumor-induced angiogenesis and implicates ILT4 as an important target for blocking CRC growth and metastasis. In a recent study, ILT4 and HLA-G overexpression in clear cell renal cell carcinoma (ccRCC) upregulated the levels of VEGF-C, another VEGF family member for angiogenesis [30]. Although mechanistically different, this study shed light on ILT4-modulated angiogenesis in ccRCC. In addition, in our effort to explore the underlying mechanisms for ILT4-induced CRC angiogenesis, we established a causative link between MAPK/ERK activation, VEGF-A/FGF-1 expression, and CRC angiogenesis. These studies underscore the potential pathways to block angiogenesis and disease progression in CRC patients.

In conclusion, ILT4 is enriched in tumor cells from CRC tissues, predicting higher microvessel density and poorer patient outcomes. ILT4 promoted proliferation and migration of endothelial cells *in vitro*, and tumor angiogenesis *in vivo*. Mechanistically, ILT4 activated the phosphorylation of ERK signaling, which subsequently upregulated VEGF-A and FGF-1 expression, leading to CRC angiogenesis. Furthermore, using tumor transplantation and treatment models, we demonstrated that ILT4 inhibition impeded CRC angiogenesis and progression, and improved the efficacy of Bevacizumab. Our work has provided strong evidence for ILT4-regulated tumor angiogenesis, explored the underlying mechanism in the

process, and highlighted a novel combination therapy that may overcome Bevacizumab resistance in CRC patients.

Acknowledgements

We thank Yuan Ma and Ling Wang of the Department of Pathology, Jinan Central Hospital, Shandong University, for helping with the collection of CRC samples and preparing tissue sections. This work was partially supported by grants from Shandong Provincial Natural Science Foundation (ZR2021MH268), National Natural Science Foundation of China (82103340 and 81902919), the 70th China Postdoctoral Science Foundation (2021M700054), the Jinan Science and Technology Innovation Program of Clinical Medicine (202134041), and the Shandong Province Science and Technology Development Program (202103030672).

Disclosure of conflict of interest

The authors declare that the research was conducted in the absence of any commercial or financial relationships that could be construed as a potential conflict of interest.

Address correspondence to: Dr. Yuping Sun, Phase I Clinical Study Center, Shandong Cancer Hospital and Institute, Shandong First Medical University and Shandong Academy of Medical Science, No. 440 Jiyan Road, Jinan 250117, Shandong, P. R. China. Tel: +86-13370582181; E-mail: sunyuping@live.cn

References

[1] Sung H, Ferlay J, Siegel RL, Laversanne M, Soerjomataram I, Jemal A and Bray F. Global cancer statistics 2020: GLOBOCAN estimates of incidence and mortality worldwide for 36 cancers in 185 countries. CA Cancer J Clin 2021; 71: 209-249.

[2] Siegel RL, Miller KD, Goding Sauer A, Fedewa SA, Butterly LF, Anderson JC, Cercek A, Smith RA and Jemal A. Colorectal cancer statistics, 2020. CA Cancer J Clin 2020; 70: 145-164.

[3] Folkman J and Shing Y. Angiogenesis. J Biol Chem 1992; 267: 10931-10934.

[4] Rmali KA, Puntis MC and Jiang WG. Tumour-associated angiogenesis in human colorectal cancer. Colorectal Dis 2007; 9: 3-14.

[5] Mody K, Baldeo C and Bekaii-Saab T. Antiangiogenic therapy in colorectal cancer. Cancer J 2018; 24: 165-170.

[6] Riechelmann R and Grothey A. Antiangiogenic therapy for refractory colorectal cancer: current options and future strategies. Ther Adv Med Oncol 2017; 9: 106-126.

[7] Fanger NA, Cosman D, Peterson L, Braddy SC, Maliszewski CR and Borges L. The MHC class I binding proteins LIR-1 and LIR-2 inhibit Fc receptor-mediated signaling in monocytes. Eur J Immunol 1998; 28: 3423-3434.

[8] Gao A, Sun Y and Peng G. ILT4 functions as a potential checkpoint molecule for tumor immunotherapy. Biochim Biophys Acta Rev Cancer 2018; 1869: 278-285.

[9] Lu N, Li Y, Zhang Z, Xing J, Sun Y, Yao S and Chen L. Human Semaphorin-4A drives Th2 responses by binding to receptor ILT-4. Nat Commun 2018; 9: 742.

[10] Chen HM, van der Touw W, Wang YS, Kang K, Mai S, Zhang J, Alsina-Beauchamp D, Duty JA, Mungamuri SK, Zhang B, Moran T, Flavell R, Aaronson S, Hu HM, Arase H, Ramanathan S, Flores R, Pan PY and Chen SH. Blocking immunoinhibitory receptor LILRB2 reprograms tumor-associated myeloid cells and promotes antitumor immunity. J Clin Invest 2018; 128: 5647-5662.

[11] Sun Y, Liu J, Gao P, Wang Y and Liu C. Expression of Ig-like transcript 4 inhibitory receptor in human non-small cell lung cancer. Chest 2008; 134: 783-788.

[12] Warnecke-Eberz U, Metzger R, Holscher AH, Drebber U and Bollschweiler E. Diagnostic marker signature for esophageal cancer from transcriptome analysis. Tumour Biol 2016; 37: 6349-6358.

[13] Carbone C, Piro G, Fassan M, Tamburrino A, Mina MM, Zanotto M, Chiao PJ, Bassi C, Scarpa A, Tortora G and Melisi D. An angiopoietin-like protein 2 autocrine signaling promotes EMT during pancreatic ductal carcinogenesis. Oncotarget 2015; 6: 13822-13834.

[14] Shao H, Ma L, Jin F, Zhou Y, Tao M and Teng Y. Immune inhibitory receptor LILRB2 is critical for the endometrial cancer progression. Biochem Biophys Res Commun 2018; 506: 243-250.

[15] Gao A, Liu X, Lin W, Wang J, Wang S, Si F, Huang L, Zhao Y, Sun Y and Peng G. Tumor-derived ILT4 induces T cell senescence and suppresses tumor immunity. J Immunother Cancer 2021; 9: e001536.

[16] Chen X, Gao A, Zhang F, Yang Z, Wang S, Fang Y, Li J, Wang J, Shi W, Wang L, Zheng Y and Sun Y. ILT4 inhibition prevents TAM- and dysfunctional T cell-mediated immunosuppression and enhances the efficacy of anti-PD-L1 therapy in NSCLC with EGFR activation. Theranostics 2021; 11: 3392-3416.

[17] Li J, Gao A, Zhang F, Wang S, Wang J, Wang J, Han S, Yang Z, Chen X, Fang Y, Jiang G and Sun Y. ILT3 promotes tumor cell motility and angiogenesis in non-small cell lung cancer. Cancer Lett 2021; 501: 263-276.
[18] Folkman J. Angiogenesis: an organizing principle for drug discovery? Nat Rev Drug Discov 2007; 6: 273-286.
[19] Siveen KS, Prabhu K, Krishnankutty R, Kuttikrishnan S, Tsakou M, Alali FQ, Dermime S, Mohammad RM and Uddin S. Vascular endothelial growth factor (VEGF) signaling in tumour vascularization: potential and challenges. Curr Vasc Pharmacol 2017; 15: 339-351.
[20] Liang S, Ristich V, Arase H, Dausset J, Carosella ED and Horuzsko A. Modulation of dendritic cell differentiation by HLA-G and ILT4 requires the IL-6–STAT3 signaling pathway. Proc Natl Acad Sci U S A 2008; 105: 8357-8362.
[21] Siegel RL, Miller KD and Jemal A. Cancer statistics, 2019. CA Cancer J Clin 2019; 69: 7-34.
[22] Xie YH, Chen YX and Fang JY. Comprehensive review of targeted therapy for colorectal cancer. Signal Transduct Target Ther 2020; 5: 22.
[23] Haibe Y, Kreidieh M, El Hajj H, Khalifeh I, Mukherji D, Temraz S and Shamseddine A. Resistance mechanisms to anti-angiogenic therapies in cancer. Front Oncol 2020; 10: 221.
[24] Colonna M, Samaridis J, Cella M, Angman L, Allen RL, O'Callaghan CA, Dunbar R, Ogg GS, Cerundolo V and Rolink A. Human myelomonocytic cells express an inhibitory receptor for classical and nonclassical MHC class I molecules. J Immunol 1998; 160: 3096-3100.
[25] Zhang P, Guo X, Li J, Yu S, Wang L, Jiang G, Yang D, Wei Z, Zhang N, Liu J and Sun Y. Immunoglobulin-like transcript 4 promotes tumor progression and metastasis and up-regulates VEGF-C expression via ERK signaling pathway in non-small cell lung cancer. Oncotarget 2015; 6: 13550-13563.
[26] Liu X, Yu X, Xie J, Zhan M, Yu Z, Xie L, Zeng H, Zhang F, Chen G, Yi X and Zheng J. ANGPTL2/LILRB2 signaling promotes the propagation of lung cancer cells. Oncotarget 2015; 6: 21004-21015.
[27] Cai Z, Wang L, Han Y, Gao W, Wei X, Gong R, Zhu M, Sun Y and Yu S. Immunoglobulinlike transcript 4 and human leukocyte antigenG interaction promotes the progression of human colorectal cancer. Int J Oncol 2019; 54: 1943-1954.
[28] Lapeyre-Prost A, Terme M, Pernot S, Pointet AL, Voron T, Tartour E and Taieb J. Immunomodulatory activity of VEGF in cancer. Int Rev Cell Mol Biol 2017; 330: 295-342.
[29] De Palma M, Biziato D and Petrova TV. Microenvironmental regulation of tumour angiogenesis. Nat Rev Cancer 2017; 17: 457-474.
[30] Garcia M, Palma MB, Verine J, Miriuka S, Inda AM, Errecalde AL, Desgrandchamps F, Carosella ED and Tronik-Le Roux D. The immune-checkpoint HLA-G/ILT4 is involved in the regulation of VEGF expression in clear cell renal cell carcinoma. BMC Cancer 2020; 20: 624.
[31] Niu G and Chen X. Vascular endothelial growth factor as an anti-angiogenic target for cancer therapy. Curr Drug Targets 2010; 11: 1000-1017.

Table S1. Specific primers used in this work

Target genes	Forward	Reverse
GAPDH	GGAGCGAGATCCCTCCAAAAT	GGCTGTTGTCATACTTCTCATGG
ILT4	GCATCTTGGATTACACGGATACG	CTGACAGCCATATCGCCCTG
MMP9	TGTACCGCTATGGTTACACTCG	GGCAGGGACAGTTGCTTCT
VEGF-A	AGGGCAGAATCATCACGAAGT	AGGGTCTCGATTGGATGGCA
VEGF-C	TGGCAACATAACAGAGAACAGG	CAAACTCCTTCCCCACATCTAT
VEGF-D	ACTCAGTGCAGCCCTAGAGAA	GAACACGTTCACACAAGGGG
FGF-1	GTGGATGGGACAAGGGACAG	GGCAGGGGGAGAAACAAGAT
FGF-2	AGAAGAGCGACCCTCACATCA	CGGTTAGCACACACTCCTTTG
ANGPTL-1	CAACAGTGTCCTTCAGAAGCAGC	CCAGCTTGATATACATCTGCACAG
ANGPTL-2	AACTTTCGGAAGAGCATGGAC	CGAGTCATCGTATTCGAGCGG
ANGPTL-5	CTGTATGTGGCTTTGGAATCTG	CGGTCTTGTTATGGAGGTGACT
PDGF-B	CTCGATCCGCTCCTTTGATGA	CGTTGGTGCGGTCTATGAG
PDGF-D	GCGGCTTCACTCTCAGGAGAAT	CTTGTGTCCACACCATCGTCCT

Table S2. Specific antibodies used in this work

Antibodies	Source	Identifier	Applications
Anti-ILT4	Origene	Cat.No.TA323297	IHC (1:200)
Anti-ILT4	Immuno Way	Cat.No.B9501	WB (1:1000)
Anti-GAPDH	Proteintech	Cat.No.60004-1-Ig	WB (1:5000)
Anti-VEGF-A	Abcam	Cat.No.ab9570	Neutralizing (1.2 μg/ml)
Anti-VEGF-A	Proteintech	Cat.No.66828-1-Ig	WB (1:1000)
Anti-FGF-1	Bio-techne	Cat.No.AF232	Neutralizing (10 μg/ml)
Anti-FGF-1	Abcam	Cat.No.ab9588	WB (1:1000)
Anti-ERK1/2	Cell Signaling Technology	Cat.No.4695	WB (1:1000)
Anti-phospho-ERK1/2	Abcam	Cat.No.ab201015	WB (1:1000)
Anti-SAPK/JNK	Cell Signaling Technology	Cat.No.9252	WB (1:1000)
Anti-phospho-JNK1/2/3	Abcam	Cat.No.ab124956	WB (1:1000)
Anti-P38 MPAK	Cell Signaling Technology	Cat.No.8690	WB (1:1000)
Anti-phospho- P38	Abcam	Cat.No.ab178867	WB (1:1000)
Anti-mTOR	Cell Signaling Technology	Cat.No.2983	WB (1:1000)
Anti-phospho-mTOR	Cell Signaling Technology	Cat.No.5536	WB (1:1000)
Anti-NF-κB P65	Cell Signaling Technology	Cat.No.8242	WB (1:1000)
Anti-phospho-NF-κB P65	Cell Signaling Technology	Cat.No.3033	WB (1:1000)
Anti-VEGF-A	GeneTex	Cat.No.GTX102643	IHC (1:500)
Anti-FGF-1	Abnova	Cat.No.H00002246-M02	IHC (1:200)
Anti-CD34	Maxim	Cat.No.kit-0004	IHC
Anti-ERK1/2	Proteintech	Cat.No.16443-1-AP	IHC (1:200)
Anti-phospho-ERK1/2	Abcam	Cat.No.ab32538	IHC (1:200)
Anti-NF-KB P65	Proteintech	Cat.No.10745-1-AP	IHC (1:200)
Anti-phospho-NF-kB P65	ABclonal	Cat.No.AP0123	IHC (1:200)